Journal of Membrane Science 454 (2014) 505–515

Contents lists available at ScienceDirect

Journal of Membrane Science

journal homepage: www.elsevier.com/locate/memsci

Comparison of membrane fouling at constant flux and constant transmembrane pressure conditions

Daniel J. Miller, Sirirat Kasemset, Donald R. Paul, Benny D. Freeman *

Department of Chemical Engineering, Center for Energy and Environmental Resources, and Texas Materials Institute, The University of Texas at Austin, 200 E. Dean Keeton Street, Stop C0400, Austin, TX 78712, USA

ARTICLE INFO

Article history:
Received 23 June 2013
Received in revised form
15 November 2013
Accepted 11 December 2013
Available online 19 December 2013

Keywords:
Constant flux
Constant transmembrane pressure
Threshold flux
Critical flux
Fouling
Ultrafiltration

ABSTRACT

Membrane fouling is often characterized in the laboratory by flux decline experiments, where an increase in transport resistance due to accumulation of foulants on and/or in a membrane is manifested as a decrease in permeate flux with filtration time at fixed transmembrane pressure. However, many industrial microfiltration and ultrafiltration applications operate at constant permeate flux, and there are few reports comparing these modes of operation. In this study, emulsified oil fouling of polysulfone ultrafiltration membranes was studied using both constant permeate flux and constant transmembrane pressure experiments. Mass transfer resistance changes during fouling were compared between constant flux experiments and constant transmembrane pressure experiments performed at an initial flux equal to the flux imposed during the constant flux experiment. At low fluxes, the transport resistance and its change with permeate volume per unit area agreed within experimental error regardless of operational mode. In contrast, at high fluxes, the change in membrane resistance with permeate volume per unit area was much higher in constant flux than in constant transmembrane pressure experiments. The threshold flux, defined recently as the flux at which the rate of fouling begins to increase rapidly, separates the regimes of good and poor agreement between the two types of experiments. The weak form of the critical flux, below which spontaneous adsorption is the only significant resistance imposed by foulant, was also observed.

1. Introduction

Emulsified oil is ubiquitous in wastewater streams from petroleum production and refining, metalworking, hydraulic fracturing, manufacturing, and other industrial operations [1]. Microfiltration and ultrafiltration systems utilizing polymeric membranes can produce high-quality permeate and provide a low-energy, small-footprint alternative to traditional separation techniques [1]. Unfortunately, fouling is a pervasive problem in water purification membranes [2–4]. Such membranes are frequently made of hydrophobic polymers via phase-inversion processes in which water is used as the nonsolvent [4], so hydrophobic wastewater components, such as oils, tend to aggressively foul membranes, necessitating: (1) increased energy expenditure or larger membrane area to maintain productivity, (2) frequent membrane cleaning, and (3) membrane replacement [5].

Laboratory-based membrane fouling studies are often accomplished by challenging the membrane with a model or realistic foulant solution at fixed transmembrane pressure (TMP) [6–10]. As the membrane fouls, permeate flux declines. This flux decline means that the hydrodynamic conditions at the membrane surface change with time during the experiment [11]. To address this point, some authors studied membrane fouling at constant permeate flux [12–18], where the flow of feed solution through the membrane is more constant than in fixed TMP studies [11]. Constant flux operation provides an operational mechanism by which fouling may be abated [14]. The severe fouling observed at the start of a constant TMP experiment, which occurs because of often very high initial flux (i.e., low initial membrane mass transfer resistance) of the clean membrane, is reduced by imposing a constant, and much lower, flux in constant flux operation [18]. Additionally, most industrial microfiltration and ultrafiltration applications operate at constant flux [19,20].

Although both constant flux and constant TMP studies have been reported, there are few direct comparisons of membrane fouling under both operational modes. In their work describing the critical flux concept, Field et al. provided qualitative observations of constant TMP and constant flux measurements [15]. They observed that the total mass transfer resistance of the membrane and foulant was generally low for constant flux experiments and high for constant TMP experiments, presumably due to the rapid fouling at the beginning of constant TMP experiments. Marshall,

* Corresponding author. Tel.: +1 512 232 2803.
E-mail address: freeman@che.utexas.edu (B.D. Freeman).

0376-7388/$ - see front matter © 2013 Elsevier B.V. All rights reserved.
http://dx.doi.org/10.1016/j.memsci.2013.12.027

Munro, and Trägårdh developed a crossflow system capable of operating in constant flux or constant TMP modes [21]. They filtered skimmed milk with both ultrafiltration and microfiltration membranes. Although their study focused mainly on a comparison of ultrafiltration and microfiltration fouling, they also identified experimental conditions where ultrafiltration membrane resistances developed similarly in constant flux and constant TMP fouling studies. Decloux et al. considered the operation of ultrafiltration and microfiltration membranes under both control modes, finding that constant flux operation resulted in less severe fouling than constant TMP operation, resulting in reduced cleaning frequency [20]. A few publications, including two recent reports [22,23], have focused on methods for predicting the fouling propensity of certain solutions and have, to this end, evaluated fouling at both constant flux and constant TMP. Kanani and Ghosh developed a model to predict permeate flux decline in constant TMP operation by assuming that the flux decline is comprised of many sequential constant flux steps [24]. Model parameters were obtained from constant flux experiments, which offer an unchanging hydrodynamic environment at the membrane surface, facilitating the capture of data related to concentration polarization and fouling phenomena. Further investigation of fouling phenomena at constant flux and constant TMP is, however, warranted. As noted by Sioutopoulos and Karabelas, "uncertainty exists as to whether the more common constant-pressure UF and RO laboratory tests provide fouling resistances representative of conditions prevailing in the constant flux mode of commercial plant operation" [23].

In this report, we compare constant flux and constant TMP fouling of ultrafiltration membranes being used to filter an emulsified oil solution. The resistance to permeation, which increases due to foulant accumulation on the membrane [21], is calculated as a function of the permeate volume per unit membrane area. Experiments were performed such that the initial flux in a constant TMP test was equal to the flux imposed in the corresponding constant flux test (and, consequently, the initial TMP in the constant flux experiment was equal to the TMP imposed throughout the constant TMP experiment). Agreement between the experimental protocols was good at low fluxes but not at high fluxes. The threshold flux, as recently defined by Field and Pearce [25], was found to separate the flux regime of good agreement from that of poor agreement.

2. Background

The permeate flux through a porous membrane is often described as the applied transmembrane pressure driving force, TMP, divided by the resistance to mass transfer, R, and the permeate viscosity, μ [15,25]:

$$J = \frac{\mathrm{TMP}}{\mu R} \tag{1}$$

For pure water filtration, R will represent the resistance to mass transfer associated with the clean membrane. During a fouling experiment, the resistance to permeation increases due to various mechanisms, such as pore plugging, cake layer formation, concentration polarization, osmotic pressure, etc. [26]. The total resistance to mass transfer is often described by a resistance-in-series model. In this way, the total resistance is described by individual resistances, such as the resistance of the membrane itself, the resistance due to adsorption fouling, and the resistances due to reversible and irreversible fouling. For clarity, "adsorption fouling" refers to the spontaneous adsorption of foulant to the membrane surface that occurs even under zero flux conditions. "Reversible fouling" and "irreversible fouling" refer to the accumulation of foulant that is brought to the membrane during operation; that is, when the permeate flux is greater than zero. Therefore, in reversible and irreversible fouling, as defined here, foulant is brought to the membrane primarily by convection associated with the permeate flux [11,14,18]. In constant TMP operation, the increase in R causes permeate flux to decline; in constant flux operation, TMP increases as R increases. Therefore, the change in resistance during fouling provides a convenient benchmark for comparing constant flux and constant TMP experimental results.

If the flux is sufficiently low, mechanisms such as Brownian diffusion, shear-induced diffusion, axial transport along the surface, and inertial lift can act to remove foulant particles as they reach the membrane surface due to permeate flow [18,27]. Under these conditions, the total resistance remains constant, and the permeate flux scales linearly with TMP. At somewhat higher fluxes, the aforementioned foulant removal mechanisms cannot overcome the inexorable flow of foulant towards the membrane surface, so foulant accumulates on, and perhaps in, the membrane during filtration, and the resistance increases with time. The flux no longer scales linearly with TMP and, eventually, a limiting flux is reached where further increases in TMP do not produce increases in flux [4].

Field et al. introduced the concept of critical flux—the maximum flux that can be achieved with slight or negligible fouling—to distinguish the regime of invariant resistance from that where resistance changes with flux [15]. The exact value of the critical flux depends upon foulant properties (e.g., concentration and particle size), membrane properties (e.g., pore size and material), and crossflow velocity [28]. Two forms of the critical flux are further defined: the strong form and the weak form [28]. At fluxes below the strong form of the critical flux, the only contribution to R is that of the clean, unfouled membrane itself; i.e., fouling does not contribute to the resistance to permeation [25]:

$$J = \frac{\mathrm{TMP}}{\mu R_m} \quad \text{for } J < J_{cs} \tag{2}$$

where J is the flux, TMP is the transmembrane pressure, R_m is the membrane resistance, and J_{cs} is the flux associated with the strong form of the critical flux. For the weak form of the critical flux, the resistance to permeation is given by the sum of the membrane resistance and resistance from adsorption of foulant to the membrane surface [25]:

$$J = \frac{\mathrm{TMP}}{\mu(R_m + R_{ads})} \quad \text{for } J < J_{cw} \tag{3}$$

where R_{ads} is the resistance due to adsorption, and J_{cw} is the weak form of the critical flux. The resistance due to adsorption reflects foulant whose adsorption to the membrane occurs spontaneously and independently of flux [25]. Therefore, whether a particular membrane/foulant system exhibits the strong form of the critical flux or the weak form of the critical flux is dictated by whether or not foulant adsorption to the membrane is a significant contributor to resistance. Because such adsorption occurs spontaneously and independently of flux (and even in the absence of flux) [25], a membrane/foulant system will show either the strong form or the weak form of the critical flux, but not both.

At fluxes above the two forms of the critical flux, the resistance to permeation is increased due to reversible and irreversible fouling [25]:

$$J = \frac{\mathrm{TMP}}{\mu(R_m + R_{rev} + R_{irrev})} \quad \text{for } J > J_{cs} \tag{4}$$

$$J = \frac{\mathrm{TMP}}{\mu(R_m + R_{ads} + R_{rev} + R_{irrev})} \quad \text{for } J > J_{cw} \tag{5}$$

where R_{rev} is the resistance due to reversible fouling, and R_{irrev} is the resistance due to irreversible fouling. As noted previously, R_{rev} and R_{irrev} refer to resistances due to permeation-driven fouling of the membrane.

A third form of the critical flux, the critical flux for irreversibility, has also been described. It refers to the flux at which the feed fluid irreversibly transforms from a dispersed phase to aggregates on the membrane surface, triggered by flux-induced concentration enhancement [28]. Once such aggregation occurs, the original membrane properties may only be recovered by cleaning or other protocols [28]. This phenomenon was not experimentally evaluated here, so the critical flux for irreversibility will not be discussed.

The definitions of the weak and strong forms of the critical flux require that the total resistance not vary with time at fluxes below the critical flux. However, in some cases, a constant resistance during filtration may never be achieved, even at extremely low fluxes. LeClech et al. reported a scenario in which a zero rate of TMP increase with time was never observed during constant flux microfiltration of sewage, so a critical flux could not be identified. They did observe, however, a regime of linearity in the TMP/flux relationship at low fluxes, and deviation from linearity at high fluxes. In the regime of linearity, the (non-zero) rate of fouling was constant at several low fluxes. In the regime of non-linearity, the rate of fouling increased with increasing flux. The threshold flux has recently been defined as the flux at which the rate of fouling significantly increases [25]. The threshold flux and the critical flux are, therefore, conceptually similar, since below either of them, the TMP scales linearly with flux, and above either of them, the rate of fouling increases appreciably. Experimentally, flux stepping protocols, which will be described later, can be used to identify the threshold or critical flux. However, a threshold flux can be distinguished from a critical flux by observing the rate of fouling below the flux in question. If TMP does not increase with time, the identified flux is a critical flux; if the transmembrane pressure slowly rises at the same rate, even at low fluxes, the flux is a threshold flux [25].

3. Materials and methods

3.1. Membranes and foulant

Flat-sheet PS-20 polysulfone UF membranes were obtained from Sepro Membranes, Inc. (Oceanside, CA). These membranes have a nominal pure water permeance of 900 LMH/bar and molecular weight cutoff of 20,000 Da. The roll of membrane material was stored in a cool, dry, dark place. Before use, 4 cm × 9 cm sample coupons were cut from the sheet. Ethanol was used to wet the porous structure of the membranes. Sample coupons were carefully placed, selective face down, in a dish containing ethanol so that they floated atop the ethanol for several seconds before sinking; this technique permitted air to escape through the nonwoven backing (exposed to the atmosphere) as ethanol wicked into the pores. This procedure helped minimize trapping of air in the pores of the membrane, which could contribute to variability in membrane permeance. After soaking in ethanol for 24 h, samples were transferred to ultrapure water for at least 1 h to exchange the ethanol. The coupons were not permitted to dry after initial wetting.

The foulant used in this study was an emulsion of soybean oil in water. Soybean oil (Wesson) was purchased from a local supermarket and DC193, which is a silicone-based, non-ionic surfactant, was obtained from Dow Corning (Midland, MI). The emulsion was prepared by combining oil and surfactant in a 9:1 ratio with enough ultrapure water to produce an overall emulsion concentration of 1500 ppm (1350 ppm soybean oil, 150 ppm surfactant). Emulsification was performed in a Waring laboratory blender (Torrington, CT) operated at 20,000 rpm for 180 s. Fresh emulsion was prepared immediately prior to each fouling experiment. The ultrapure water used in all of these studies was produced by a Millipore Milli-Q Advantage A10 water purification system (18.2 MΩ-cm at 25 °C, 1.2 ppb TOC) (Billerica, MA). The average oil droplet diameter was about 1.5 μm, with nearly all droplets in the range of 0.8–3.0 μm [29].

3.2. Constant transmembrane pressure fouling experiments

Constant TMP fouling experiments were performed in a manner similar to those reported previously [5,30–34]. The crossflow system employed was based on one purchased from Separations Systems Technologies (San Diego, CA). A 30 L feed tank was equipped with a heating coil connected to a water bath to maintain the feed temperature at 25 °C. A diaphragm pump from Texas Pump and Equipment (Wichita Falls, TX) was used to pump the feed solution through three stainless steel membrane sample cells in series. The feed flow rate was monitored using an oval gear flow meter from Brooks Instrument (Hatfield, PA). Single-ended pressure transducers from Omega Engineering (Stamford, CT) were used to monitor the feed and reject pressures. A backpressure regulator (BPR) from Equilibar (Fletcher, NC) was installed downstream of the three membrane sample cells. An electronic air regulator from Proportion Air, Inc. (McCordsville, IN) was mounted to the BPR and adjusted the BPR pressure based on readings from the feed pressure transducer by a LabVIEW program incorporating proportional/integral feedback control. The retentate was continuously recycled to the feed tank.

Permeate from each sample cell was collected in a large beaker on an electronic mass balance. The change in mass was recorded as a function of time, and the permeate flux was calculated as follows:

$$J = \frac{\Delta M}{\rho_w A \Delta t} \tag{6}$$

where J is the flux, ΔM is the mass of permeate collected during a time period of Δt, ρ_w is the density of water, and A is the filtration area (19.4 cm^2). A differential pressure transducer (Omega Engineering) measured the difference between the feed and permeate pressures of each sample cell. A backpressure regulator (Equilibar) and electronic air regulator (Proportion Air, Inc.) was installed on each permeate line. In a scheme similar to that employed to control feed pressure, each permeate line BPR was operated in feedback control using the TMP reading from its respective differential pressure transducer. In this way, the TMP applied over each membrane was carefully and independently controlled. The TMP feedback control and data collection, including mass of the permeate, the three transmembrane pressures, the feed pressure, and the feed flow rate, were performed by the same LabVIEW program mentioned above.

To begin a constant TMP fouling experiment, membrane sample coupons were loaded in the test cells, and the feed tank was filled with 27 L of ultrapure water. The feed pump began circulation of the water at 0.8 L/min, corresponding to a crossflow velocity of 0.18 m/s and a Reynolds number of approximately 1000 inside the flow channel of each test cell (Reynolds number was calculated by assuming that the flow channel consists of two parallel plates with large aspect ratios) [32]. The feed pressure was 2.1 barg (30 psig) in all experiments, and the TMP across each sample cell was adjusted to produce a desired pure water flux. During startup with pure water operation, the recycled retentate water was continuously filtered using a Matrikx CTO Plus® activated carbon cartridge filter from KX Technologies (West Haven, CT) to remove contaminants that might foul the membrane. The importance of continuous feed filtration during pure water permeation has been discussed elsewhere [32]. The membranes were operated with ultrapure water for a few minutes to

ensure that all air was purged from the permeate lines. The manufacturer specifies a water permeance of 900 LMH/bar; dead end filtration tests revealed a permeance range of approximately 600–1300 LMH/bar for small samples cut from the membrane roll. Typically, if the membranes were operating with ultrapure water near the middle of this range, e.g., 800–1000 LMH/bar, the experiments were continued. If not, then the membranes were replaced, and the experiment was re-started.

Membrane fouling was initiated by adding 3 L of concentrated soybean oil emulsion to the 27 L of ultrapure water already in the feed tank sufficient to produce a 1500 ppm overall concentration, as described in Section 3.1. The activated carbon cartridge filter was bypassed just before adding the foulant solution. As the membranes fouled, their flux decreases were tracked by the electronic balances. The total organic carbon (TOC) content of permeate and feed samples was measured by a Total Organic Carbon Analyzer from Shimadzu Scientific (Japan) to determine membrane rejection. The rejection was calculated as follows:

$$\Re = \left(1 - \frac{C_p}{C_f}\right) \times 100\% \tag{7}$$

where $\Re$ is the rejection, C_p is the organic carbon concentration in the permeate, and C_f is the organic carbon concentration in the feed.

3.3. Constant flux fouling experiments

The construction and operation of the crossflow system employed in constant flux fouling experiments is described in detail elsewhere [35]. The principle difference between the constant flux and constant TMP systems was the replacement of the permeate line BPR′s in the constant TMP system with peristaltic pumps (Cole Parmer, Vernon Hills, IL) in the constant flux system. These pumps regulated the permeate flow and, in turn, the flux. Additionally, due to the occlusion of the tubing by the pump head rollers, the pumps isolated the pressure on the downstream face of the membrane from the atmosphere, enabling accurate measurement of changes in the TMP with differential pressure transducers (Omega Engineering). The pressure on the feed side of the membrane was held constant and, as the membrane fouled and the membrane resistance increased, the pressure on the permeate side of the membrane decreased, resulting in an increase in TMP. In the case of extreme fouling, the permeate pressure decreased to atmospheric pressure, and the TMP became equal to the gauge feed pressure. In these instances, the experiment was terminated to prevent the permeate pressure from falling below atmospheric pressure, which invited the formation of air bubbles in the permeate line that could disrupt an accurate measurement of permeate flux. A Coriolis-style flow meter (Bronkhorst, Bethlehem, PA) was installed on each permeate line. As in the constant TMP system, a LabVIEW program was used to collect data and control instruments.

Constant flux fouling experiments were started by loading membrane coupons in the sample cells. The feed pump (Cole Parmer) and backpressure regulator (Equilibar) were automatically controlled at the desired feed flow rate of 0.8 L/min (corresponding to a crossflow velocity of 0.18 m/s and a Reynolds number of 1000 inside the cell flow paths) and a feed pressure of 2.1 barg (30 psig), respectively. At the beginning of an experiment, ultrapure water was circulated through the system. The permeate pump speeds were adjusted to produce the desired flux from each membrane cell just before fouling was started; if the membranes were not operating with pure water in the range of 800–1000 LMH/bar at this time, the experiment was stopped, and the membrane coupons were replaced. During ultrapure water permeation at system startup, an activated carbon cartridge filter was used to continuously filter the recycled feed water to minimize any membrane fouling by trace residual foulant in the system. Unlike the constant TMP system, the constant flux system had two 8 L feed tanks, so fouling was initiated by bypassing the cartridge filter and switching the feed to the tank containing 8 L of 1500 ppm soybean oil emulsion foulant solution, prepared as described in Section 3.1. During fouling, the permeate flow meters were used to ensure that rigorously constant flux was maintained; pump speeds were automatically adjusted through a feedback control scheme. Membrane rejection was calculated as described for the constant TMP experiments.

In addition to fouling experiments where the same flux was imposed for the entire run, the constant flux system was also used to perform flux stepping experiments to determine the membrane threshold flux [14,16,36]. During fouling, the membrane was initially operated at a low flux (e.g., 5 LMH) for 10 min. After 10 min, the flux was increased to 10 LMH, and the membrane operated for another 10 min. In this manner, the flux was gradually increased by 5 LMH at 10-min intervals until a flux of 105 LMH was reached, where very rapid fouling was observed.

3.4. Measurement of permeance change due to foulant adsorption

The effect of foulant adsorption on membrane permeance was measured following a procedure proposed by Field and Pearce [25]. Membranes were operated at 40 LMH in the constant flux crossflow system with ultrapure water as the feed for 60 min to measure the pure water permeance. The permeate pumps were then turned off, resulting in zero permeate flux. Soybean oil emulsion was fed to the membranes for 1 h with no permeation. After 1 h, the feed was switched back to ultrapure water and permeate pump operation resumed to produce a flux of 40 LMH for 10 min. The pure water permeance was again measured.

4. Results and discussion

4.1. Critical and threshold flux determination

The critical and threshold fluxes of the PS-20 UF membrane were evaluated using a well-known flux-stepping protocol [16]. The result of the flux stepping experiment is shown in Fig. 1.

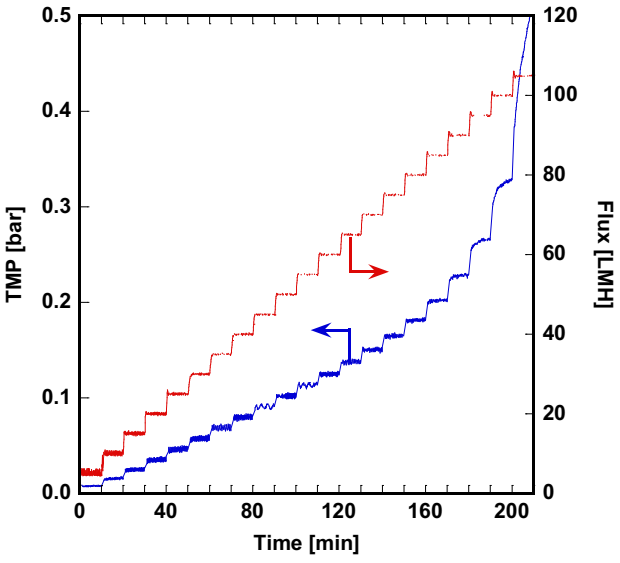

Fig. 1. Flux stepping experiment with PS-20 UF membrane and 1500 ppm soybean oil emulsion foulant. The flux was gradually increased in 10-min, constant-flux intervals from 5 to 105 LMH. The TMP was recorded during each flux. Feed pressure: 2.1 barg, crossflow velocity: 0.18 m/s.

Fig. 2 presents the *average* TMP, calculated as the arithmetic mean of all transmembrane pressures recorded over each constant flux interval shown in Fig. 1, as a function of imposed permeate flux. TMP_{avg} vs. flux plots are frequently used to determine critical and threshold fluxes from flux stepping experiments [14,16,35]. Three linear regressions are drawn through the TMP_{avg} values, labeled A, B, and C. Most of the TMP_{avg} values, corresponding to the flux range of 15–60 LMH, lie on regression line B. At fluxes higher than 60 LMH, the slope of the TMP_{avg}/flux relationship progressively increases with increasing flux. Regression line C was drawn to find the flux at which this change in slope occurs. The flux increases nonlinearly in region C, so only the first two points beyond region B were used to fit the line identified as *C* in Fig. 2. At the lowest fluxes tested, 5 and 10 LMH, TMP_{avg} values deviated from regression line *B*. Regression line *A* was drawn through these two points; regression line A also intersects the origin (*i.e.*, zero flux at zero TMP). The intersections of such linear regressions, where the slopes of the regressions change, typically correspond to the critical [14,16] or threshold [35] fluxes. Here, the intersection of regression lines A and B was identified as the weak form of the critical flux (J_{cw}), and the intersection of regression lines B and C was the threshold flux; the methods used to make these determinations will be described in the following discussion.

The strict definitions of the strong and weak forms of the critical flux require that no change in resistance occur with time at fluxes below either form of the critical flux [25]. Therefore, below the critical flux, the TMP must remain constant even as the membrane is filtering a potentially fouling feed solution. If the TMP is increasing with time, the resistance is also increasing, and the membrane is operating above the critical flux. At fluxes below the threshold flux, however, the resistance (and, therefore, TMP) may increase at a slow, constant rate with time [25]. TMP profiles were carefully evaluated, especially at the lowest fluxes considered. Fig. 3 presents the TMP profiles recorded over the first 60 min of the flux stepping experiment shown in full in Fig. 1. At fluxes of 5 and 10 LMH, the TMP profiles are reasonably constant, suggesting that the resistance was not increasing with time. Therefore, the flux where regression lines A and B intersect (cf., Fig. 2) is a critical flux. Since the definitions of both the strong and weak forms of the critical flux require that the TMP remain constant with time, this flux could not be identified as either the strong form or the weak form based only on the lack of change of TMP with time.

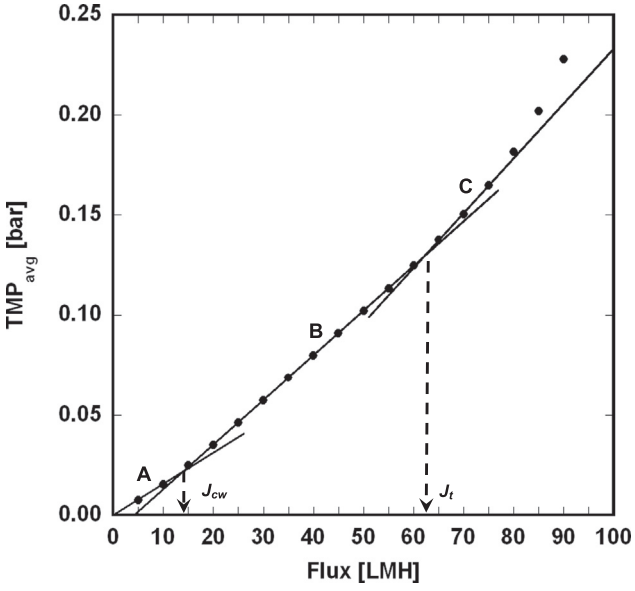

Fig. 2. Critical and threshold flux determination from flux stepping experiment shown in Fig. 1. TMP_{avg} was calculated as the arithmetic mean of all transmembrane pressures recorded during each flux step. Based upon the slope of the TMP_{avg}/flux relationship, the data were separated into three regions, denoted as A, B, and C. The intersection of regression lines A and B is the weak form of the critical flux (J_{cw}), while the intersection of regression lines B and C is the threshold flux (J_t).

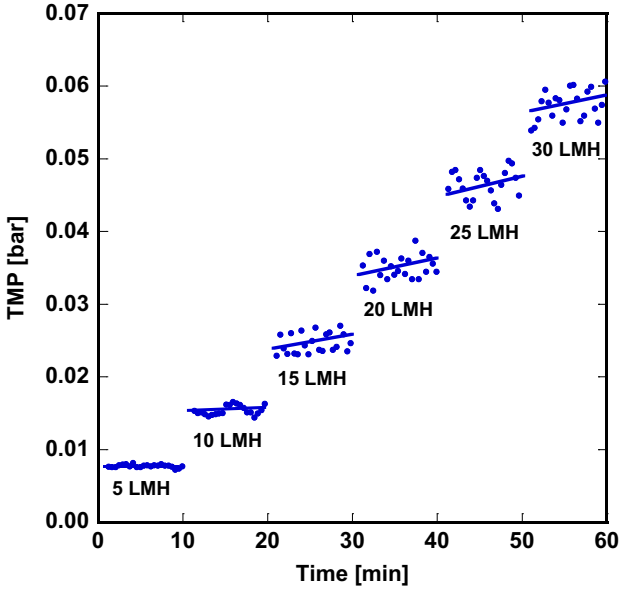

Fig. 3. Detail of TMP profiles from Fig. 1 at low fluxes. Although the TMP profiles at fluxes below 62 LMH appear to be invariant with time in Fig. 1, close inspection reveals that the TMP is gradually increasing over each constant flux interval at fluxes of 15 LMH and greater. As noted by Field and Pearce [24], such a result suggests that 62 LMH is a threshold flux (Fig. 2), and 14 LMH is the weak form of the critical flux (Fig. 2). Lines drawn to guide the eye.

At fluxes greater than 10 LMH, the TMP slowly increased with time over each 10 minute constant flux interval, as shown in Fig. 3. Furthermore, the rate of TMP increase appeared similar regardless of flux, suggesting that the rate of fouling was similar at all fluxes. As shown by the linear relationship between TMP_{avg} and flux in regression line B (*cf.*, Fig. 2), the rate of fouling appears to remain constant up to a flux of 62 LMH. At fluxes higher than 62 LMH, the slope of the TMP_{avg}/flux relationship increases, suggesting an increase in the rate of fouling. Since the threshold flux distinguishes a regime of relatively slow, constant fouling from a regime of more rapid fouling [25], 62 LMH is identified as the threshold flux (J_t).

Although a relatively recent concept, the threshold flux has been determined by similar use of a TMP_{avg}/flux plot by Le Clech et al. [36]. In their study of a membrane bioreactor using a similar flux stepping protocol, a time-invariant TMP was never achieved, but the average TMP over each interval scaled linearly with flux at low fluxes. At higher fluxes, the slope of the average TMP vs. flux relationship increased. Le Clech et al. identified a critical flux where this slope change occurred, but they acknowledged that the strict requirement for unchanging TMP with time was not met. In a later discussion of Le Clech's report, Field and Pearce suggested that the term "threshold flux" be used to resolve this ambiguity [25]. Other techniques historically used for critical flux determination, such as pressure cycling [37], have been adapted to determine threshold fluxes [38]. Although similar techniques have been used to determine critical and threshold fluxes, few authors have observed both in the same system. Luo et al., for example, observed both the threshold flux and a critical flux for irreversibility in their study of shear-enhanced nanofiltration of dairy effluent [39].

To determine whether the critical flux shown in Fig. 2 (14 LMH) is the strong form or the weak form, the effect of foulant

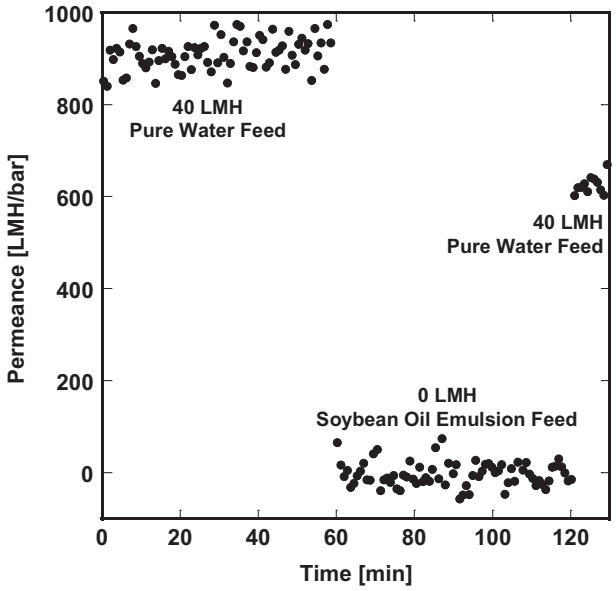

Fig. 4. Experimental determination of the decrease in permeance due to foulant adsorption. The PS-20 UF membrane was operated with pure water at 40 LMH for 60 min to establish a baseline permeance of 900 LMH/bar. Foulant was adsorbed to the membrane in the absence of convective flow through the membrane by reducing the flux to zero and switching the feed to soybean oil emulsion for 60 min. Operation at 40 LMH was resumed with pure water feed for 10 min to measure the permeance after foulant adsorption. Feed pressure: 2.1 barg, crossflow velocity: 0.18 m/s.

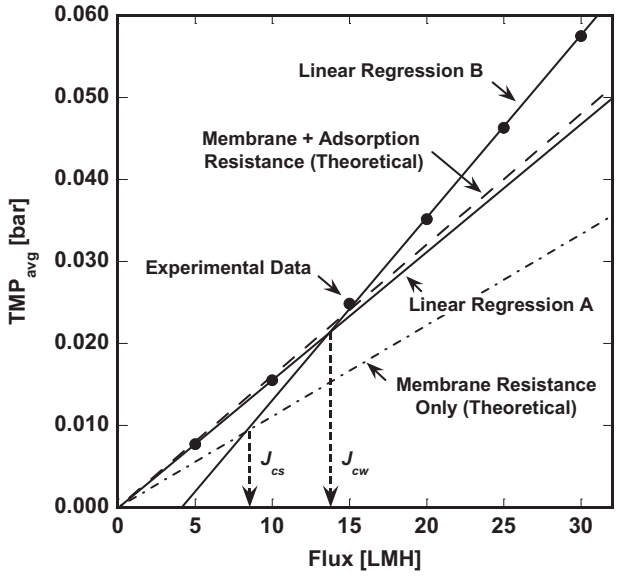

Fig. 5. Detail of the TMP_{avg}/flux relationship from Fig. 2 at low fluxes. TMP_{avg} values derived from the flux stepping experiment presented in Fig. 3 are shown along with the linear regressions A and B (i.e., the solid lines) through those data above and below the weak form of the critical flux (J_{cw}). The TMP_{avg}/flux relationships are also shown for the hypothetical fouling scenarios where the resistance is identical to that of a clean membrane (the line labeled Membrane Resistance Only) and the resistance accounts for spontaneous foulant adsorption to the membrane (the line labeled Membrane+Adsorption Resistance). It is proposed that the strong and weak forms of the critical flux may be identified as shown.

adsorption to the membrane in the absence of permeate flow was evaluated as described in Section 3.3. Results are shown in Fig. 4. After exposing the membrane to foulant under conditions of zero permeate flux, the membrane permeance decreased from 900 LMH/bar to 625 LMH/bar. By evaluating fouling under zero permeate flux conditions, the resistance increase due to adsorption, which occurs spontaneously in the absence of permeate flux, was separated from that of reversible and irreversible foulant accumulation due to convective flow of foulants to the membrane surface [25].

Fig. 5 presents TMP_{avg} values as a function of flux at low fluxes. Experimental data are shown as filled circles, while the linear regressions A and B (also shown in Fig. 2) are solid lines. These regressions are compared with membrane behavior under two hypothetical fouling scenarios. First, if no foulant adsorption occurs and no foulant accumulates on the membrane due to convective flow towards the surface, the only resistance will be that of the membrane itself. This scenario is represented by the dot-dashed line labeled "Membrane Resistance Only". This line was drawn based on the membrane pure water permeance of 900 LMH/bar. Membrane operation along this line when challenged with a fouling feed suggests that the membrane is operating below the strong form of the critical flux, because, as described in the background section, the only resistance to permeation at fluxes below the strong form of the critical flux is due to that of the membrane. In this definition, foulant adsorption or reversible and irreversible accumulation due to convection are not significant contributors to resistance. None of the experimental data lie along this operational line, so the strong form of the critical flux was not observed.

The second hypothetical fouling scenario is represented by the dashed line labeled "Membrane+Adsorption Resistance". This operational line is based on the result of the experiment shown in Fig. 4, where adsorption of foulant to the membrane surface is a significant contributor to resistance. The dashed line was drawn based on a permeance of 625 LMH/bar, the permeance after adsorption of foulant at zero flux conditions. The experimental data at 5 and 10 LMH nearly lie directly on the dashed line and, therefore, linear regression A (623 LMH/bar) is essentially equal to it. Thus, during filtration of the soybean oil emulsion at 5 and 10 LMH, the membrane and foulant adsorption to the membrane are the major contributors to resistance. Substantial accumulation of foulant due to convective flow towards the membrane likely does not occur at these low fluxes. As noted in the background section, spontaneous foulant adsorption, but not permeate-driven accumulation of foulant, is permitted at fluxes below the weak form of the critical flux. Due to the invariant TMP profiles at 5 and 10 LMH (*cf.*, Fig. 3), and the close correlation of experimental fouling behavior with the hypothetical scenario representing foulant adsorption only, 14 LMH (*i.e.*, the intersection of lines A and B on Figs. 4 or 5) is likely the weak form of the critical flux.

That the weak form of the critical flux was observed suggests that foulant adsorption is a significant contributor to resistance in this membrane/foulant system. If foulant adsorption had not been significant, it is proposed that the strong form of the critical flux would have been observed, and TMP_{avg} at 10 LMH would have been on linear regression B, and the TMP_{avg} at 5 LMH would have been on the dot-dashed line (*cf.*, Fig. 5). Regardless of which form of the critical flux was observed, the fact that linear regression B does not pass through the origin suggests that permeation-driven foulant accumulation must not be a dominant fouling mechanism at very low fluxes.

4.2. Constant flux fouling

Constant flux fouling experiments were performed at five fluxes: 25, 40, 55, 85, and 100 LMH, representing two fluxes above and three fluxes below the estimated threshold flux of 62 LMH. The TMP evolution at each flux is presented in Fig. 6. As the imposed flux increased, the TMP increased, as expected. This result is reasonable from the perspective of the both the initial TMP and the TMP during fouling. With increasing flux, the initial TMP (the TMP observed during pure water filtration) increased in proportion to the membrane resistance. During fouling, higher fluxes

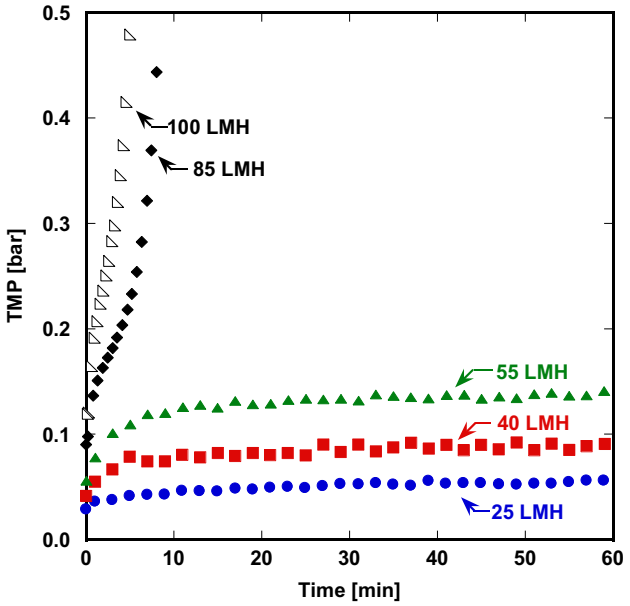

Fig. 6. TMP evolution of PS-20 UF membranes during constant flux fouling with a 1500 ppm soybean oil emulsion feed. Membranes operated below the threshold flux of 62 LMH exhibited low and slowly increasing TMP's, but those operated above the threshold flux exhibited rapidly increasing TMP's. The curves shown are representative of at least three replicates at each flux. Feed pressure: 2.1 barg, crossflow velocity: 0.18 m/s.

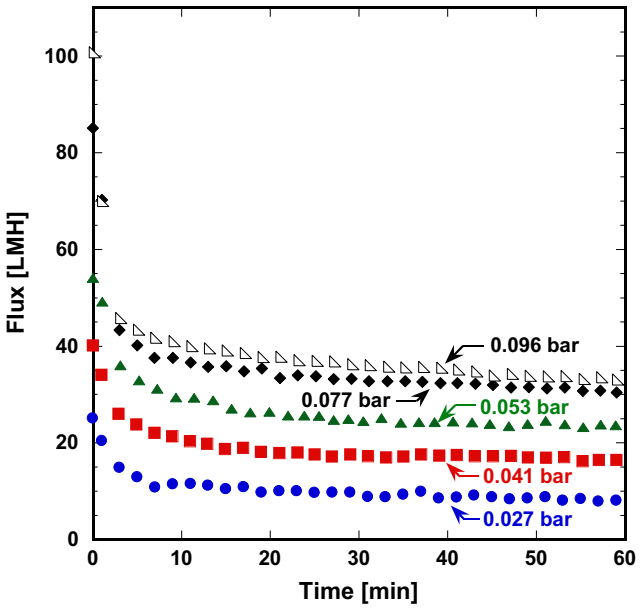

Fig. 7. Flux decline during constant TMP fouling of PS-20 UF membranes with a 1500 ppm soybean oil emulsion feed. Membranes were operated at five transmembrane pressures sufficient to produce initial fluxes identical to those imposed in the constant flux fouling experiment (cf., Fig. 6). All curves show qualitatively similar behavior, regardless of whether the initial flux was above or below the threshold flux. The curves shown are representative of at least three replicates at each TMP. The numbers in the figure represent the TMP for each fouling experiment.

brought greater amounts of the emulsified oil foulant to the membrane surface, increasing foulant accumulation on the membrane. A significant qualitative difference existed in fouling behavior, however, between the membranes operated above and below the threshold flux. Membranes operated at 25, 40, and 55 LMH (i.e., below the threshold flux) showed a modest increase in TMP in the first few minutes and slowly increasing TMP thereafter. The early TMP rise was likely due to a combination of concentration polarization and a short period of rapid fouling [24,40]. Marshall, Munro, and Trägårdh found that, even at extremely low fluxes, some fouling of ultrafiltration membranes could not be prevented during start-up [41]. The TMP increase at the start of fouling, where the TMP profile is concave down, is indicative of concentration polarization development and some rapid initial fouling, but it does not suggest extensive fouling that would preclude long-term operation. The slow, linear TMP rise after this initial period of rapid fouling may correspond to a pore blockage fouling mechanism [42].

The membranes operated at fluxes of 85 and 100 LMH, both well above the threshold flux, showed rapid fouling. Above the threshold flux, foulants were brought to the membrane surface more rapidly than they could be removed by crossflow shear forces and diffusion. TMP profiles of a similar shape have been reported by others, where the TMP exhibited a dramatic upturn during fouling and, thereafter, increased rapidly [42–47]. The upturn in the TMP profile likely corresponded to the onset of cake formation [42], which sharply increased the resistance to water transport through the membrane [47]. To maintain the constant permeate flux condition, the TMP increased concomitant with the increase in resistance. Foulants continued to accumulate on the cake, and the resistance continued to rise until the experiment was stopped when the TMP reached the maximum measureable value (2.1 bar).

4.3. Constant transmembrane pressure fouling

Constant TMP fouling was performed at five transmembrane pressures: 0.027, 0.041, 0.053, 0.077, and 0.096 bar. These TMP values were chosen because they produced initial membrane fluxes identical to those imposed during the constant flux experiments (e.g., a TMP of 0.027 bar produced an initial flux of 25 LMH, *etc.*). Regardless of whether the initial flux was above or below the threshold flux, the flux decline curves exhibited qualitatively similar behavior, as shown in Fig. 7. Membranes with initial fluxes below the threshold flux (i.e., TMP=0.027, 0.041, and 0.053 bar) experienced modest degrees of fouling. The two membranes with initial fluxes above the threshold flux (i.e., TMP=0.077 and 0.096 bar) fouled quickly to fluxes below the threshold flux. Once at these lower fluxes, the fouling rate decreased, and the flux profiles flattened. Due to the extremely low transmembrane pressures required to produce initial fluxes of 5 and 10 LMH (below the weak form of the critical flux), limitations in accuracy of the back pressure regulators on the permeate lines in the constant TMP system did not allow us to study constant TMP fouling below the weak form of the critical flux.

4.4. Comparison of constant flux and constant transmembrane pressure fouling

From the experimental results in the constant flux and constant TMP experiments, the resistance to mass transfer, R, was calculated according to Eq. (1). Because the organic rejection of these membranes was very high ($>98\%$, as discussed later), the permeate viscosity was assumed equal to that of pure water at 25 °C (*i.e.*, 8.95×10^{-4} Pa s [48]). The resistance values were plotted as a function of the permeate volume normalized by the total filtration area. In the constant TMP experiment, the flux changed with time and, as a result, the rate at which foulant was brought to the membrane surface changed with time. In contrast, the constant flux experiment brought a steady rate of foulant to the membrane surface for the entire experimental duration. By plotting the resistance as a function of permeate volume/area, the resistances may be compared at points where the same amount of permeate has been produced in each experiment (i.e., the membranes have

filtered the same amount of feed). Resistances from constant flux experiments were compared to resistances from constant TMP experiments started at the same flux imposed during the constant flux experiment. The typical pure water permeance of the membrane was 900 LMH/bar, so the initial resistance (recorded during pure water filtration just before fouling was initiated) was around $4.4 \times 10^{11}\ m^{-1}$.

Fig. 8 presents resistance comparisons between constant flux and constant TMP fouling at fluxes below the threshold flux (i.e., 62 LMH). Constant flux experiments were performed at 25, 40, and 55 LMH, and constant TMP experiments were performed at 0.027, 0.041, and 0.053 bar, corresponding to initial fluxes of 25, 40, and 55 LMH, respectively. Within experimental error, the resistances during constant flux and constant TMP fouling were indistinguishable. Experimental error was greatest for experiments at the lowest flux due to the low transmembrane pressures required and the uncertainty in the differential pressure transducer readings at the low end of their span. In all three cases, the resistance increased at low permeate volumes and approached a plateau thereafter. Regardless of the applied flux or TMP, all membranes reached a similar resistance of about $1.0 \times 10^{12}\ m^{-1}$. Since all membranes were operating below their threshold flux, foulant accumulation did not contribute strongly to increased membrane resistance as the applied (initial) flux increased. A similar result was observed by Aimar et al., where increasing the flux did not greatly impact the observed resistance during constant flux filtration of whey protein using polysulfone ultrafiltration membranes [11].

Fig. 9 presents the resistances developed during constant flux and constant TMP experiments at (initial) fluxes above the threshold flux (*i.e.,* 62 LMH). Constant flux experiments were performed at 85 and 100 LMH. Constant TMP experiments at 0.076 and 0.097 bar produced initial fluxes of 85 and 100 LMH, respectively. Unlike the experiments at (initial) fluxes below the threshold flux, fouling above the threshold flux produced different behavior in constant flux and constant TMP operation. In the constant TMP case, initial fluxes above the threshold flux caused rapid fouling and, consequently, a sharp decline in permeate flux (*cf.*, Fig. 7), which manifests itself as an increase in resistance at low permeate volume/area (V/A) (*e.g.*, < 1 cm). After the flux fell below the threshold flux, the rate of fouling diminished, and little change in membrane resistance was observed thereafter. In constant flux fouling above the threshold flux, a brief period of relatively slow fouling was observed, which closely matched the resistance development in the constant TMP experiment over this same period. However, in the constant flux case, a rapid escalation in resistance was observed near $V/A = 1$ cm. Because the flux in the constant TMP experiment rapidly fell well below the threshold flux, the hydrodynamic forces responsible for bringing foulant to

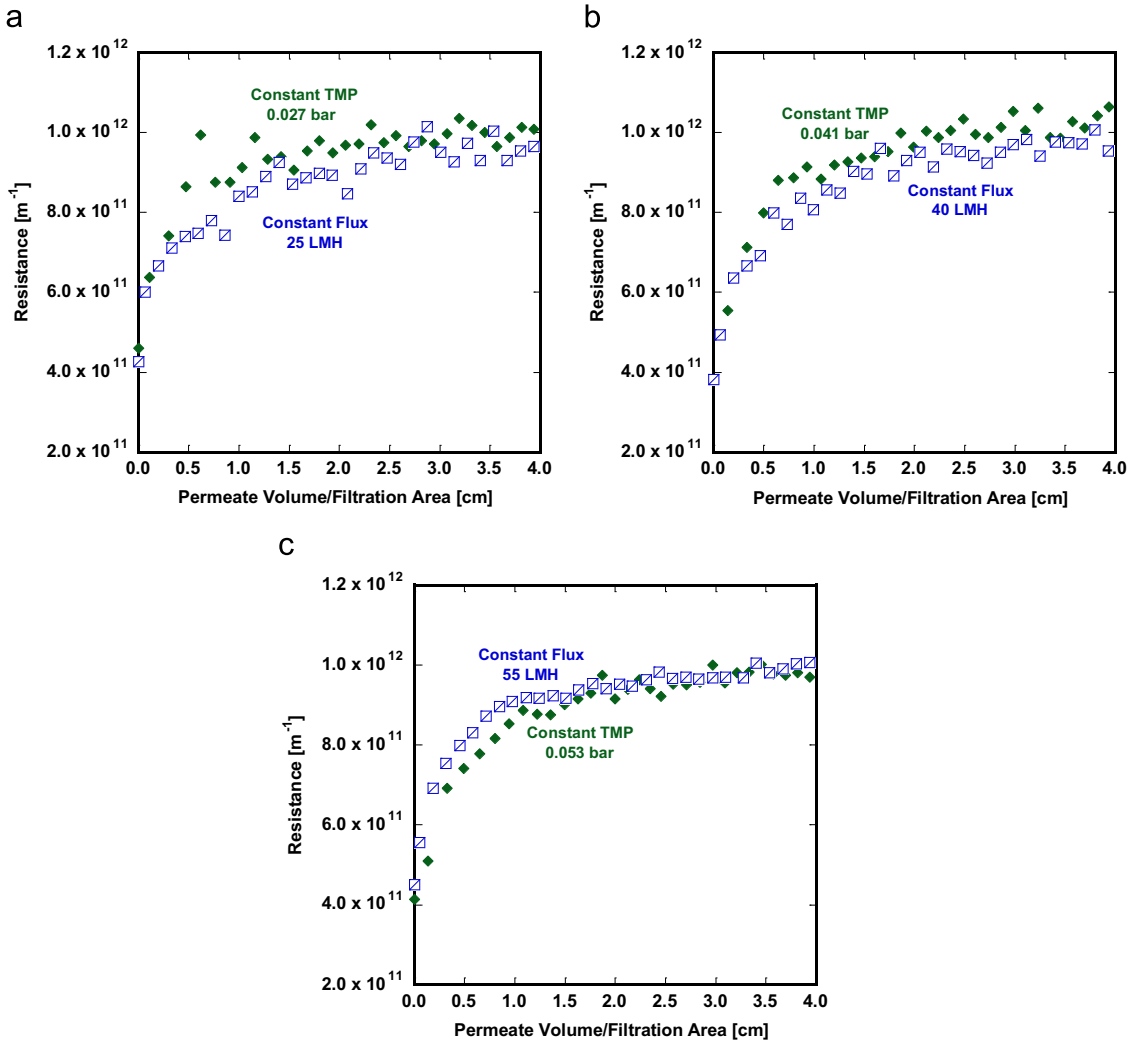

Fig. 8. Comparisons of mass transfer resistance evolution during constant flux and constant TMP experiments at fluxes below the threshold flux (i.e., 62 LMH), calculated from data shown in Figs. 6 and 7 using Eq. (1). (a) Constant flux =25 LMH, constant TMP=0.027 bar (initial flux=25 LMH). (b) Constant flux=40 LMH, constant TMP=0.041 bar (initial flux=40 LMH). (c) Constant flux=55 LMH, constant TMP=0.053 bar (initial flux=55 LMH).

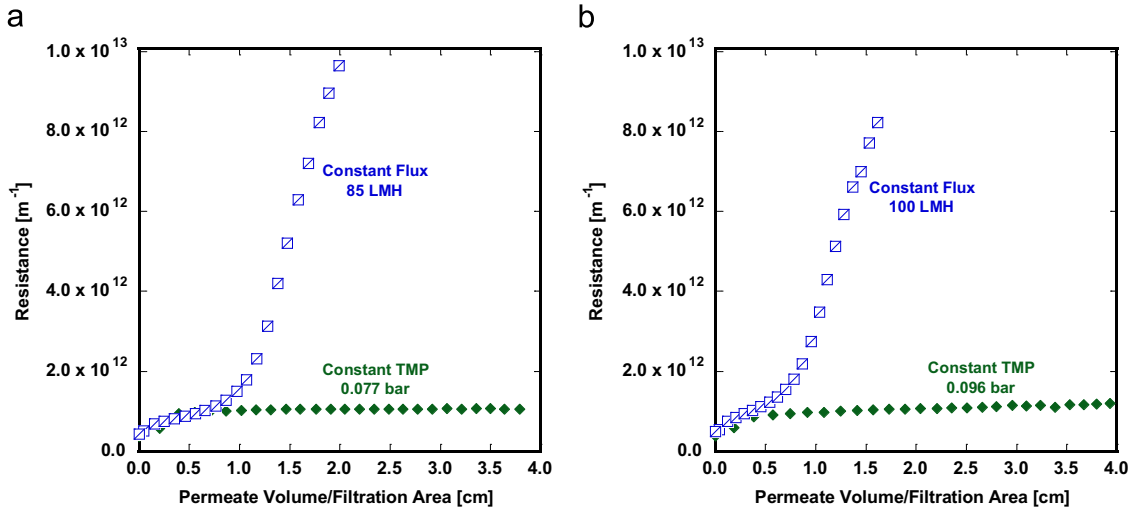

Fig. 9. Comparisons of resistance evolution during constant flux and constant TMP experiments at fluxes above the threshold flux (62 LMH), calculated from data shown in Figs. 6 and 7 using Eq. (1). (a) Constant flux = 85 LMH, constant TMP = 0.077 bar (initial flux = 85 LMH). (b) Constant flux = 100 LMH, constant TMP = 0.096 bar (initial flux = 100 LMH).

and from the membrane surface were able to balance, resulting in no further changes in resistance with continuing permeation. In the case of constant flux operation, such a dynamic equilibrium could not be reached, because the high, sustained rate of permeation through the membrane caused the continued accumulation of foulant on the membrane. Similar behavior during constant flux fouling have been reported elsewhere [42–47]. Others have suggested that such an upturn in resistance corresponds to the beginning of cake formation on the membrane surface. For example, Ho and Zydney suggested that pore blockage was the major fouling mechanism during the slow, steady increase in resistance initially observed during constant flux protein microfiltration [42]. After the pores were substantially blocked, a cake layer began to form, rapidly driving up the resistance [42]. Ognier et al. proposed a similar hypothesis in their study of constant flux microfiltration of bioreactor effluent [47]. During constant flux filtration under these conditions, the fouling appears to be a self-accelerating phenomenon. As pores gradually become blocked by foulant, the local flux in neighboring pores must increase to maintain the same flux over the entire filtration area. This increase in local flux draws foulant more quickly into the remaining open pores, causing them to foul more quickly. Once many pores are blocked and the local flux is sufficiently high, cake formation begins, dramatically increasing the resistance [47]. Due to this rapid fouling and cake formation under constant flux operation, the membrane TMP values reached the gauge feed pressure after a short time and the experiment was terminated, meaning that constant flux resistance data stopped at permeate volume/area values less than approximately 2 cm.

Most industrial ultrafiltration and microfiltration systems are operated at constant flux, which permits a consistent rate of permeate production [19,20]. Additionally, depending upon the character of the feed water, the flux may be adjusted to maximize water production while minimizing fouling. Decloux et al. showed that, in ultrafiltration, membranes were more productive with fewer cleanings when operated in constant flux mode than when operated in constant TMP mode [20]. Clearly, however, such benefits may only be realized below the threshold flux, because constant flux operation above the threshold flux appears to be unsustainable. At the very least, constant flux operation at high fluxes would require frequent backwashing or membrane cleaning. Flux optimization protocols, which have been discussed elsewhere, may be used to better understand the most desirable flux (*e.g.*, the "sustainable flux") for long-term industrial operation [20,25]. Sustainable flux determination involves many factors beyond those explored here, including membrane, energy, and cleaning costs [25].

Table 1
Organic rejection during constant flux and constant TMP fouling experiments. Rejections were calculated based on the total organic carbon analysis of permeate and feed. Fluxes shown refer to initial fluxes in the case of constant TMP experiments. Values shown are averages of at least three replicate trials, and errors are standard deviations of those averages.

Flux (LMH)	*Rejection during constant flux filtration (%)*	*Rejection during constant TMP filtration (%)*
25	98.9 ± 0.4	98.5 ± 0.1
40	98.3 ± 0.1	98.4 ± 0.1
55	98.4 ± 0.2	98.3 ± 0.1
85	99.0 ± 0.3	97.7 ± 0.1
100	99.0 ± 0.1	97.7 ± 0.1

Organic rejection measurements for all fouling experiments, including both constant flux and constant TMP tests, are shown in Table 1. In the constant TMP experiments, the rejection decreased overall from 98.5% to 97.7% as initial flux (and TMP) increased. This decline in rejection is well known in ultrafiltration. With increasing TMP, the accumulation of foulant on the membrane surface also increased, exacerbating concentration polarization and, therefore, increasing organic permeation through the membrane [4]. For constant flux fouling, the rejection also decreased as flux increased from 25 LMH to 40 LMH; the rejections at 40 LMH and 55 LMH could not be statistically distinguished. However, an increase in rejection was observed as the flux was increased from 55 LMH (below the threshold flux) to 85 LMH (above the threshold flux). A minimum in rejection may exist at 55 LMH, the flux closest to the threshold flux of 62 LMH. A similar result was reported by Chan et al., where a rejection minimum was observed near the critical flux during protein filtration using regenerated cellulose ultrafiltration membranes [49]. Below the threshold flux, concentration polarization was enhanced with increasing flux, as in the case of constant TMP fouling, causing a decrease in rejection. At sustained fluxes above the threshold flux, substantial accumulation of foulant on the membrane surface may have hindered organic permeation through the membrane, counteracting the effects of increased concentration polarization at 85 and 100 LMH. Therefore, the rejection increased with increasing flux above the threshold flux [50].

5. Conclusions

Fouling of polysulfone ultrafiltration membranes by an emulsified oil feed was studied under constant permeate flux and constant TMP operations. The weak form of the critical flux and the threshold flux were determined by flux stepping. Constant flux fouling was performed at fluxes above and below the threshold flux. Below the threshold flux, modest increases in TMP were observed. Above the threshold flux, fouling was severe, and the TMP rapidly increased. Constant TMP experiments were performed at pressures that produced initial fluxes equal to the fluxes imposed in the constant flux experiments. Regardless of whether the initial flux was above or below the threshold flux, all constant TMP experiments showed qualitatively similar behavior. Constant flux and constant TMP experiments were compared by plotting total resistance as a function of permeate volume/area. At (initial) fluxes below the threshold flux, the resistances as a function of permeate volume/area in both modes of operation were indistinguishable within experimental error. Above the threshold flux, the constant TMP resistance rose initially but reached a plateau because the flux fell rapidly to a value below the threshold flux and fouling lessened in severity. The resistance during constant flux fouling rose to the same value at which the constant TMP resistance reached a plateau, but thereafter rapidly increased. Organic rejection decreased with increasing initial flux (increasing TMP) in the case of constant TMP experiments, probably due to enhanced concentration polarization at high transmembrane pressures. Similarly, the organic rejection decreased with increasing flux during constant flux filtration at fluxes below the threshold flux. Above the threshold flux, the rejection increased, likely due to restricted permeation through substantial foulant accumulation on the membrane surface.

Acknowledgments

The authors acknowledge financial support from the National Science Foundation Graduate Research Fellowship Program (0648993) and the National Science Foundation Science and Technology Center for Layered Polymeric Systems (DMR-0423914) as well as CBET 1160069.

References

[1] J. Mueller, Y. Cen, R.H. Davis, Crossflow microfiltration of oily water, J. Membr. Sci. 129 (2) (1997) 221–235.
[2] H. Ju, B.D. McCloskey, A.C. Sagle, V.A. Kusuma, B.D. Freeman, Preparation and characterization of crosslinked poly(ethylene glycol) diacrylate hydrogels as fouling-resistant membrane coating materials, J. Membr. Sci. 330 (1–2) (2009) 180–188.
[3] A.C. Sagle, H. Ju, B.D. Freeman, M.M. Sharma, PEG-based hydrogel membrane coatings, Polymer 50 (3) (2009) 756–766.
[4] R.W. Baker, Membrane Technology and Applications, 2nd ed., John Wiley & Sons, West Sussex, England, 2004.
[5] H. Ju, B.D. McCloskey, A.C. Sagle, Y.-H. Wu, V.A. Kusuma, B.D. Freeman, Crosslinked poly(ethylene oxide) fouling resistant coating materials for oil/water separation, J. Membr. Sci. 307 (2) (2008) 260–267.
[6] D. Bhattacharyya, A.B. Jumawan, R.B. Grieves, L.R. Harris, Ultrafiltration characteristics of oil–detergent–water systems: membrane fouling mechanisms, Sep. Sci. Technol. 14 (6) (1979) 529–549.
[7] W.R. Bowen, Q. Gan, Properties of microfiltration membranes: flux loss during constant pressure permeation of bovine serum albumin, Biotechnol. Bioeng. 38 (7) (1991) 688–696.
[8] S. Buetehorn, F. Carstensen, T. Wintgens, T. Melin, D. Volmering, K. Vossenkaul, Permeate flux decline in cross-flow microfiltration at constant pressure, Desalination 250 (3) (2010) 985–990.
[9] C.-C. Ho, A.L. Zydney, Effect of membrane morphology on the initial rate of protein fouling during microfiltration, J. Membr. Sci. 155 (2) (1999) 261–275.
[10] J. Louie, I. Pinnau, I. Ciobanu, K. Ishida, A. Ng, M. Reinhard, Effects of polyether–polyamide block copolymer coating on performance and fouling of reverse osmosis membranes, J. Membr. Sci. 280 (1–2) (2006) 762–770.
[11] P. Aimar, J.A. Howell, M. Turner, Effects of concentration boundary layer development on the flux limitations in ultrafiltration, Chem. Eng. Res. Des. 67 (3) (1989) 255–261.
[12] M. Turker, J. Hubble, Membrane fouling in a constant-flux ultrafiltration cell, J. Membr. Sci. 34 (2–3) (1987) 267–281.
[13] P.S. Beier, G. Jonsson, Critical flux determination by flux-stepping, AIChE J. 56 (7) (2010) 1739–1747.
[14] D.Y. Kwon, S. Vigneswaran, A.G. Fane, R. Ben Aim, Experimental determination of critical flux in cross-flow microfiltration, Sep. Purif. Technol. 19 (3) (2000) 169–181.
[15] R.W. Field, D. Wu, J.A. Howell, B.B. Gupta, Critical flux concept for microfiltration fouling, J. Membr. Sci. 100 (3) (1995) 259–272.
[16] K.Y.-J. Choi, B.A. Dempsey, Bench-scale evaluation of critical flux and TMP in low-pressure membrane filtration, J. Am. Water Works Assoc. 97 (7) (2005) 134–143.
[17] J.A. Howell, D. Wu, R.W. Field, Transmission of bovine albumin under controlled flux ultrafiltration, J. Membr. Sci. 152 (1) (1999) 117–127.
[18] V. Chen, A.G. Fane, S. Madaeni, I.G. Wenten, Particle deposition during membrane filtration of colloids: transition between concentration polarization and cake formation, J. Membr. Sci. 125 (1) (1997) 109–122.
[19] B. Alspach, S. Adham, T. Cooke, P. Delphos, J. Garcia-Aleman, J. Jacangelo, et al., Microfiltration and ultrafiltration membranes for drinking water, J. Am. Water Works Assoc. 100 (12) (2008) 84–97.
[20] M. Decloux, L. Tatoud, Importance of the control mode in ultrafiltration: case of raw cane sugar remelt, J. Food Eng. 44 (2) (2000) 119–126.
[21] A.D. Marshall, P.A. Munro, G. Trägårdh, The effect of protein fouling in microfiltration and ultrafiltration on permeate flux, protein retention and selectivity: a literature review, Desalination 91 (1) (1993) 65–108.
[22] L.-N. Sim, Y. Ye, V. Chen, A.G. Fane, Comparison of MFI-UF constant pressure, MFI-UF constant flux and crossflow sampler – modified fouling index ultrafiltration (CFS-MFIUF), Water Res. 45 (4) (2010) 1639–1650.
[23] D.C. Sioutopoulos, A.J. Karabelas, Correlation of organic fouling resistances in RO and UF membrane filtration under constant flux and constant pressure, J. Membr. Sci. 407–408 (2012) 34–46.
[24] D.M. Kanani, R. Ghosh, A constant flux based mathematical model for predicting permeate flux decline in constant pressure protein ultrafiltration, J. Membr. Sci. 290 (1–2) (2007) 207–215.
[25] R.W. Field, G.K. Pearce, Critical, sustainable and threshold fluxes for membrane filtration with water industry applications, Adv. Colloid Interf. Sci. 164 (1–2) (2011) 38–44.
[26] M. Taniguchi, J.E. Kilduff, G. Belfort, Modes of natural organic matter fouling during ultrafiltration, Environ. Sci. Technol. 37 (8) (2003) 1676–1683.
[27] G. Belfort, R.H. Davis, A.L. Zydney, The behavior of suspensions and macromolecular solutions in crossflow microfiltration, J. Membr. Sci. 96 (1–2) (1994) 1–58.
[28] P. Bacchin, P. Aimar, R.W. Field, Critical and sustainable fluxes: theory, experiments and applications, J. Membr. Sci. 281 (1–2) (2006) 42–69.
[29] H. Ju, Water Transport Study in Crosslinked Poly (Ethylene Oxide) Hydrogels as Fouling-Resistant Membrane Coating Materials, The University of Texas at Austin, TX, 2010.
[30] B.D. McCloskey, H.B. Park, H. Ju, B.W. Rowe, D.J. Miller, B.D. Freeman, A Bioinspired Fouling-Resistant, Surface modification for water purification membranes, J. Membr. Sci. 413–414 (2012) 82–90.
[31] A.C. Sagle, E.M. Van Wagner, H. Ju, B.D. McCloskey, B.D. Freeman, M. M. Sharma, PEG-coated reverse osmosis membranes: desalination properties and fouling resistance, J. Membr. Sci. 340 (1–2) (2009) 92–108.
[32] E.M. Van Wagner, A.C. Sagle, M.M. Sharma, B.D. Freeman, Effect of crossflow testing conditions, including feed pH and continuous feed filtration, on commercial reverse osmosis membrane performance, J. Membr. Sci. 345 (1–2) (2009) 97–109.
[33] B.D. McCloskey, H. Ju, B.D. Freeman, Composite membranes based on a selective chitosan – poly(ethylene glycol) hybrid layer: synthesis, characterization, and performance in oil – water purification, Ind. Eng. Chem. Res. 49 (1) (2010) 366–373.
[34] S. Kasemset, A. Lee, D.J. Miller, B.D. Freeman, M.M. Sharma, Effect of polydopamine deposition conditions on fouling resistance, physical properties, and permeation properties of reverse osmosis membranes in oil/water separation, J. Membr. Sci. 425–426 (2013) 208–216.
[35] D.J. Miller, D.R. Paul, B.D. Freeman, A Crossflow, Filtration system for constant permeate flux membrane fouling characterization, Rev. Sci. Instrum. 84 (3) (2013) 035003.
[36] P. Le Clech, B. Jefferson, I.S. Chang, S.J. Judd, Critical flux determination by the flux-step method in a submerged membrane bioreactor, J. Membr. Sci. 227 (1–2) (2003) 81–93.
[37] B. Espinasse, P. Bacchin, P. Aimar, On an experimental method to measure critical flux in ultrafiltration, Desalination 146 (1–3) (2002) 91–96.
[38] M. Stoller, M. Bravi, A. Chianese, Threshold flux measurements of a nanofiltration membrane module by critical flux data conversion, Desalination 315 (2013) 142–148.
[39] J. Luo, L. Ding, Y. Wan, M.Y. Jaffrin, Threshold flux for shear-enhanced nanofiltration: experimental observation in dairy wastewater treatment, J. Membr. Sci. 409–410 (2012) 276–284.
[40] R. Ghosh, Study of membrane fouling by BSA using pulsed injection technique, J. Membr. Sci. 195 (1) (2002) 115–123.
[41] A.D. Marshall, P.A. Munro, G. Trägårdh, Design and development of a cross-flow membrane rig to compare constant pressure and constant flux operation

in ultrafiltration and microfiltration, Trans. Inst. Chem. Eng. C: Food Bioprod. Process. 74 (2) (1996) 92–100.
[42] C.-C. Ho, A.L. Zydney, Transmembrane pressure profiles during constant flux microfiltration of bovine serum albumin, J. Membr. Sci. 209 (2) (2002) 363–377.
[43] Z. Cai, C. Wee, M.M. Benjamin, Fouling mechanisms in low-pressure membrane filtration in the presence of an adsorbent cake layer, J. Membr. Sci. 433 (2013) 32–38.
[44] G. Gésan, G. Daufin, U. Merin, J.-P. Labbé, A. Quémerais, Fouling during constant flux crossflow microfiltration of pretreated whey. Influence transmembrane pressure gradient, J. Membr. Sci. 80 (1) (1993) 131–145.
[45] G. Gésan, G. Daufin, U. Merin, Performance of whey crossflow microfiltration during transient and stationary operating conditions, J. Membr. Sci. 104 (3) (1995) 271–281.
[46] P. Kovalsky, G. Bushell, T.D. Waite, Prediction of transmembrane pressure build-up in constant flux microfiltration of compressible materials in the absence and presence of shear, J. Membr. Sci. 344 (1–2) (2009) 204–210.
[47] S. Ognier, C. Wisniewski, A. Grasmick, Membrane bioreactor fouling in sub-critical filtration conditions: a local critical flux concept, J. Membr. Sci. 229 (1–2) (2004) 171–177.
[48] G.N. Lewis, R.T. MacDonald, The viscosity of H^2H^2O, J. Am. Chem. Soc. 55 (1933) 4730–4731.
[49] R. Chan, V. Chen, M.P. Bucknall, Ultrafiltration of protein mixtures: measurement of apparent critical flux, rejection performance, and identification of protein deposition, Desalination 146 (1–3) (2002) 83–90.
[50] V. Chen, Performance of partially permeable microfiltration membranes under low fouling conditions, J. Membr. Sci. 147 (2) (1998) 265–278.